DIFFUSION MODELS FOR THE SQUID AXON SCHWANN CELL LAYER

ROBERT E. TAYLOR, *Laboratory of Biophysics, Intramural Research Program, National Institute of Neurological and Communicative Disorders and Stroke, National Institutes of Health, Bethesda, Maryland 20205*
FRANCISCO BEZANILLA, *Department of Physiology, Jerry Lewis Neuromuscular Research Center and Brain Research Institute, University of California, Los Angeles School of Medicine, Los Angeles, California 90024 U.S.A.*
EDUARDO ROJAS, *Department of Biophysics, School of Biological Sciences, University of East Anglia, Norwich, NR4 7TJ, Great Britain*

ABSTRACT The Schwann cell, basement membrane, and connective tissue layers that surround the squid giant axon and constitute barriers to diffusion, were modeled in a number of ways to analyze various experimental results. The experiments considered are (*a*) the time-course of the potassium concentration in the space between the Schwann cell and the axon membrane (from now on referred to as the F-H space) after an initial loading, (*b*) the time-course of sodium concentration in the F-H space after a sudden change in the sodium concentration in the external fluid; (*c*) the time-course of the concentration of tetrodotoxin (TTX) or saxitoxin (STX) in the F-H space after a sudden change in external concentration, including (or not) the effects of specific binding of TTX or STX to sites on the axon membrane and nonsaturable binding to sites in the F-H space or in the spaces (clefts) between Schwann cells; (*d*) the effects of the F-H space, clefts, and diffusion into the clefts from the outside (from now on referred to as convergence into the clefts) on the measured series resistance.

The analysis shows that (1) in no case is it necessary to include the effects of the convergence into the clefts from the outside; (2) in case *a*, the basement membrane, connective tissue layers, and the unstirred layer may be neglected, i.e., the clefts are rate limiting; (3) in case *b* the clefts may be neglected, i.e., the unstirred layer is rate limiting; (4) in most cases the clefts may be replaced by an equivalent thin diffusion barrier.

INTRODUCTION

The models for diffusion discussed in this paper were devised for and used in the analysis of the results of experiments designed to estimate the density of specific binding sites for tetrodotoxin (TTX) and saxitoxin (STX) in the squid axon membrane under conditions where sodium currents could be measured in the same axon and a value for the conductance of a single channel determined (Keynes et al., 1975). Preliminary reports have appeared (Keynes et al., 1973; Bezanilla, 1973; Keynes et al., 1974; Rojas, 1973).

The giant axon of squid is surrounded by a layer of Schwann cells, a basement membrane and connective tissues. There were early indications that these structures constituted a diffusion barrier and that this barrier was separated from the axon membrane by a small space (Shanes, et al., 1953). The possibility of potassium accumulation as the result of current flow during a depolarizing voltage clamp pulse was one of the suggestions made by Hodgkin and Huxley (1952) to explain the observation that the measured value for the potassium

reversal potential is sometimes lower than the calculated equilibrium potential. Frankenhaeuser and Hodgkin (1956) observed that the negative phase of propagated action potentials decreases during repetitive activity. They accounted for this change by assuming an accumulation of potassium ions in a small space between the axon membrane and a thin nonselective diffusion barrier with an electrical resistance of $\sim 4\ \Omega\ cm^2$. They identified this space with the space between the Schwann cell and the axon membrane and the diffusion barrier with the clefts between Schwann cells as shown in the electron micrographs of Geren and Schmitt (1954). More recent electron micrographs have expanded and clarified this picture (Villegas and Villegas, 1960*a,b,* 1968; Villegas, 1969). Frankenhaeuser and Hodgkin (1956) considered two models: (*a*) a small space between the axon and a thin diffusion barrier, for which the analysis fit the data, and (*b*) a finite diffusion layer with no space which did not fit. They suggested that a combination of the two models might also be satisfactory. Similar kinds of experiments have been done where the results are satisfactorily fit by the model with space plus thin layer (Adelman et al., 1973; unpublished analysis of data in Rojas et al., 1969), but other results cannot be fit to this model, such as the time-course of the change in resting potential after changes in external potassium concentration (Goldman, 1968; Taylor et al., 1969), the time-course of the effects of changing external calcium concentration (Rojas et al., 1969), and time-course of the washout of sodium or chloride ions from the extracellular space of squid axons (Lennon et al., 1970), and the effects of changing external sodium, TTX or STX concentrations (Keynes et al., 1973, 1975). Adam (1973) has considered a model where the clefts between the Schwann cells are considered explicitly. This is a special case of our "anatomical model," ignoring the effects of the basement membrane, connective tissue, and unstirred layer.

We should like to point out that what is here referred to as the "Frankenhaeuser-Hodgkin" space is the space between the Schwann cell layer and the axolemma, and not, as stated by Adam (1973), the "entire SCL with its system of intermembraneous spaces." Our F-H space is identical to the "Geren-Schmitt space" of Adam.

ANATOMICAL MODEL: NO CHEMICAL REACTION OR BINDING

To set up the equations for diffusion across the outer unstirred layer, the connective tissue and basement membrane, through the clefts between the Schwann cells and into the Frankenhaeuser-Hodgkin (F-H) space between the Schwann cells and the axon membrane, we shall make a number of simplifications to the geometry as indicated in Fig. 1 A. The Schwann cells are considered to be all of the same size and the clefts straightened. The length, width and distance apart of the clefts are average values which should be consistent with electron micrographic observations. The axon membrane is taken to be planar, and gradients perpendicular to the plane of the figure are ignored.

As indicated in Fig. 1 A, a plane of symmetry bisects a cleft and another bisects a Schwann cell. Therefore, only the shaded region needs to be considered in our analysis.

The F-H space and the clefts are narrow (in the range of 100–400 Å). For this reason, in Fig. 1 B we consider only unidimensional flow in regions 1 and 2 with concentrations C_1 and C_2, respectively. However, to examine the effects of diffusion convergence into the outer end of the clefts we consider bidimensional flow in the unstirred layer (region 3). Unless stated otherwise the term "unstirred layer" shall be taken to include the connective tissue and

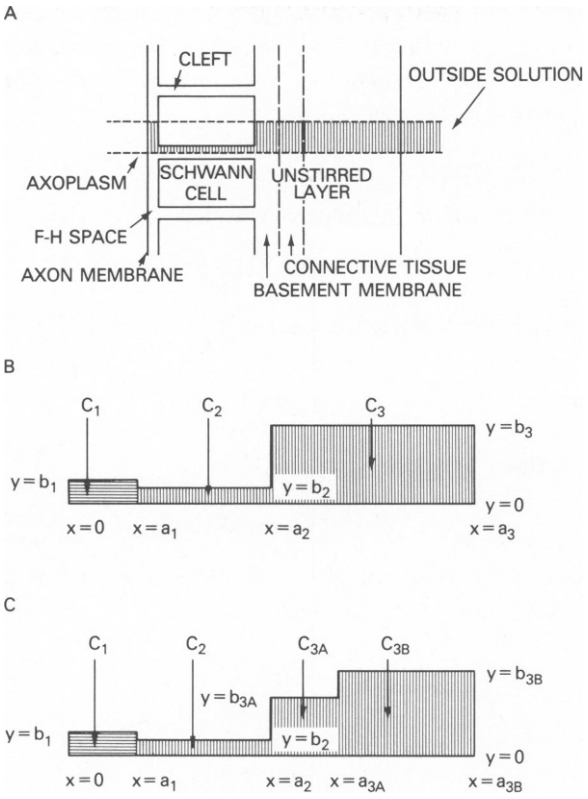

FIGURE 1 The Anatomical model. (A) Diagram of the anatomical components considered. (B) Diagram to indicate the terms used in the analysis of the anatomical model including diffusion convergence into the external openings of the clefts, but with no binding in the three regions 1, 2, and 3 with concentrations C_1, C_2, and C_3, respectively. (C) Diagram to indicate terms used in the analysis of the anatomical model neglecting diffusion convergence, but including binding in the F-H space (region 1) and nonsaturable binding in regions 1, 2, or 3A.

basement membrane. We shall change the orientation of the F-H space so that its long dimension lies along the x axis and will not assume that this region is well stirred in the x direction and derive the average concentration in this space. The geometry is shown in Fig. 1 B, divided into three regions, namely, 1 representing the F-H space, 2 representing the clefts between Schwann cells, and 3 representing the basement membrane, connective tissue, and unstirred layer. They are considered individually and connected by appropriate continuity and boundary conditions.

We want to know the average concentration in region 1, the F-H space, as a function of time $C_1(t)$ under two different conditions: (a) initially all of the regions are at the same concentration and a step change in concentration is applied outside the unstirred layer (at $x = a_3$); (b) initially the F-H space is loaded at concentration c_1, different from the concentration in the other two spaces, and the concentration at $x = a_3$ is maintained at c_{a_3}. Define

$$T = Dt, \tag{1}$$

where t is time in seconds and D is the diffusion coefficient in square centimeters per second. In regions 1 and 2 the diffusion coefficient is defined as kD, where $k \leq 1$. A bar over a variable indicates that it has been Laplace transformed with respect to T. s is the argument of the transformed function which is a complex variable.

Region 1: The F-H Space

The concentration is $C_1'(x, t)$, and for unidimensional flow

$$\partial C_1'/\partial t = kD\partial^2 C_1'/\partial x^2, \tag{2}$$

where k is a factor such that kD represents the diffusion coefficient. Let $C_1(x, T) = C_1(x, Dt) = C_1'(x, t)$ using 1,

$$\partial C_1/\partial T = k\partial^2 C_1/\partial x^2. \tag{3}$$

At $x = a_0$ we assume no flow, therefore

$$\partial C_1/\partial x|_{x=0} = 0.$$

At $x = a_1$ we assume that the concentration and the flow are equal on both sides of the boundary between regions 1 and 2. It follows that:

$$b_1 \frac{\partial C_1}{\partial x}\bigg|_{x=a_1} = b_2 \frac{\partial C_2}{\partial x}\bigg|_{x=a_1} \tag{4}$$

and

$$C_1|_{x=a_1} = C_2|_{x=a_1}, \quad t > 0. \tag{5}$$

Writing

$$C_1(x, 0) = c_1, \quad t = 0, \quad 0 \leq x \leq a_1, \tag{6}$$

the problem is specified.

Applying the Laplace transformation with respect to T to Eqs. 2–6 we have:

$$\overline{C}_1 = \frac{d\overline{C}_1}{dx}\bigg|_{a_1} \frac{\cosh \lambda' x}{\lambda' \sinh \lambda' a_1} + \frac{c_1}{s}, \tag{7}$$

where

$$\lambda' = \sqrt{s/k}. \tag{8}$$

Region 2: The Cleft between Schwann Cells

For unidimensional flow we have:

$$\frac{\partial C_2}{\partial T} = k \frac{\partial^2 C_2}{\partial x^2}, \tag{9}$$

with the boundary conditions

$$b_2 \frac{\partial C_2}{\partial x}\bigg|_{x=a_1} = b_1 \frac{\partial C_1}{\partial x}\bigg|_{x=a_1}, \tag{10}$$

and

$$b_2 k \frac{\partial C_2}{\partial x}\bigg|_{x=a_2} = \int_0^{b_3} \frac{\partial C_3}{\partial x}\bigg|_{x=a_2} dy \tag{11}$$

for

$$C_2(x, 0) = c_0, \quad t = 0, \quad a_1 \leqslant x \leqslant a_2. \tag{12}$$

Applying the Laplace transformation with respect to T to Eqs. 9–12, we have:

$$\bar{C}_2 = \frac{d\bar{C}_2}{dx}\bigg|_{a_2} \frac{\cosh \lambda'(x - a_1)}{\lambda' \sinh \lambda'(a_1 - a_2)} + \frac{dC_2}{dx}\bigg|_{a_1} \frac{\cosh \lambda'(x - a_2)}{\lambda' \sinh \lambda'(a_1 - a_2)} + \frac{c_0}{s}. \tag{13}$$

Region 3: The Basement Membrane, Connective Tissue, and Unstirred Layer

For bidimensional flow we have (using $k = 1$):

$$\frac{\partial C_3}{\partial T} = \frac{\partial^2 C_3}{\partial x^2} + \frac{\partial^2 C_3}{\partial y^2}. \tag{14}$$

With no flow across the line $y = 0$ or across the line at $y = b_3$, the boundary conditions are written as:

$$\frac{\partial C_3}{\partial y}\bigg|_{y=0} = 0, \tag{15}$$

and

$$\frac{\partial C_3}{\partial y}\bigg|_{y=b_3} = 0. \tag{16}$$

With the initial condition,

$$C_3(x, y, 0) = c_0, \quad t = 0, \tag{17}$$

and an imposed outside concentration,

$$C_3(a_3, y, t) = c_{a_3}, t > 0, \quad x = a_3. \tag{18}$$

For no flow across the Schwann cell membrane (line at $x = a_2, y > b_1$) and continuity at $x = a_2$, we have:

$$D \frac{\partial C_3}{\partial x}\bigg|_{x=a_2} = \begin{cases} 0, & y > b_2 \\ -U(t), & 0 \leqslant y \leqslant b_2, \end{cases} \tag{19}$$

where $U(t)$ is the flux per unit area from C_2 into C_3.

As before, the Laplace transform was applied to Eqs. 14–19 with respect to T, and then the Fourier transform was applied with respect to the variable y with the kernel.

$$\sqrt{\frac{2}{b_3}} \cos \frac{n\pi y}{b_3} \quad \text{for } n = 1, 2, \ldots$$

and

$$\sqrt{\frac{1}{b_3}} \quad \text{for } n = 0.$$

The solution for the Laplace transformed variable is (Özişik, 1968)

$$\bar{C}_3(x, y, s) = \frac{c_0}{s} + \frac{(c_{a_3} - c_0)\cosh\lambda(a_2 - x)}{s\cosh\lambda(a_3 - a_2)} + \frac{\bar{U}b_1\sinh\lambda(a_3 - x)}{b_3\lambda\cosh\lambda(a_3 - a_2)}$$

$$+ \sqrt{\frac{2}{b_3}}\sum_{n=1}^{\infty}\left[\frac{V\sinh\beta_n(a_3 - x)}{\beta_n\cosh\beta_n(a_3 - a_2)}\cos\frac{n\pi y}{b_3}\right] \tag{20}$$

where

$$\lambda = \sqrt{s}, \beta_n = \sqrt{s + \frac{n^2\pi^2}{b_3^2}},$$

and

$$V = \sqrt{\frac{2}{b_3}}\bar{U}\frac{b_3}{n\pi}\sin\frac{n\pi b_2}{b_3}, \tag{21}$$

To satisfy continuity at $x = a_2$ we calculate the average concentration $\langle C_3 \rangle$ at $x = a_2$, from $y = 0$ to $y = b_2$. We shall put this equal to C_2 at $x = a_2$.

$$\langle \bar{C}_3 \rangle = \frac{1}{b_2}\int_0^{b_2} \bar{C}(0, y, s)\,dy.$$

Using Eq. 20 we obtain:

$$\langle \bar{C}_3 \rangle = \frac{c_0}{s} + \frac{c_{a_3} - c_0}{s\cosh\lambda(a_3 - a_2)} + \frac{\bar{U}b_2}{b_3\lambda}\tanh\lambda(a_3 - a_2)$$

$$+ \frac{2b_3}{b_2\pi^2}\sum_{n=1}^{\infty}\bar{U}\sin^2\frac{n\pi b_2}{b_3}\cdot\frac{\tanh\beta_n(a_3 - a_2)}{\beta_n n^2}. \tag{22}$$

We may now combine Eq. 22 and 13 evaluated at $x = a_2$, and Eqs. 11, 19, 4, 5, and 7, and obtain an expression for the concentration in region C_1 (the F-H space) in terms of the initial condition of all of the regions and the boundary condition of the unstirred layer in contact with the external solution. We are interested in the average $\langle C_1 \rangle$ of this region, which is:

$$\langle \bar{C}_1 \rangle = \frac{1}{a_1}\int_0^{a_1} \bar{C}_1(x, s)\,dx, \tag{23}$$

and is given ultimately by:

$$\langle \bar{C}_1 \rangle = \frac{c_1}{s} + \frac{k(c_{a_3} - c_0)}{Aa_1 s\lambda\cosh\lambda(a_3 - a_2)} - \frac{k(c_1 - c_0)}{Aa_1 s\lambda P_1} + \frac{(c_1 - c_0)b_2\sinh(a_1 - a_2)}{a_1 b_1\lambda' s P_1}, \tag{24}$$

where

$$A = \frac{b_1}{b_2}\sqrt{k}\,\frac{P_1 \cosh \lambda'(a_2 - a_1) - 1}{\sinh \lambda'(a_2 - a_1)} + \frac{kb_1P_1}{b_3}\tanh \lambda(a_3 - a_2) + \frac{2b_3b_1kP_1P_2}{b_2^2\pi^2}, \quad (25)$$

$$P_1 = \sinh \lambda'(a_1 - a_2)\left[\cosh \lambda'(a_1 - a_2) - \frac{b_2}{b_1}\cosh \lambda' a_1\right], \quad (26)$$

$$P_2 = \sum_{n=1}^{\infty} \sin^2 \frac{n\pi b_2}{b_3}\tanh \frac{\beta_n(a_3 - a_2)}{n^2\beta_n}. \quad (27)$$

The average concentration, as a function of time, in the F-H space is obtained by inverting the Laplace transform Eq. 24. This inversion was done numerically following the procedure described by Papoulis (1957) using the trigonometrical set with the series evaluated up to 20 terms using double precision arithmetic with an IBM 360 computer (IBM Corp., White Plains, N.Y.). Later (see Discussion) this transform was inverted using the National Institutes of Health modeling laboratory system (MLAB) with the PDP-10 computer (Digital Equipment Corp., Maynard, Mass.). In the latter case the inversion technique of Stehfest (1970) was employed using 10 terms. The series Eq. 27 was summed to 100 terms for

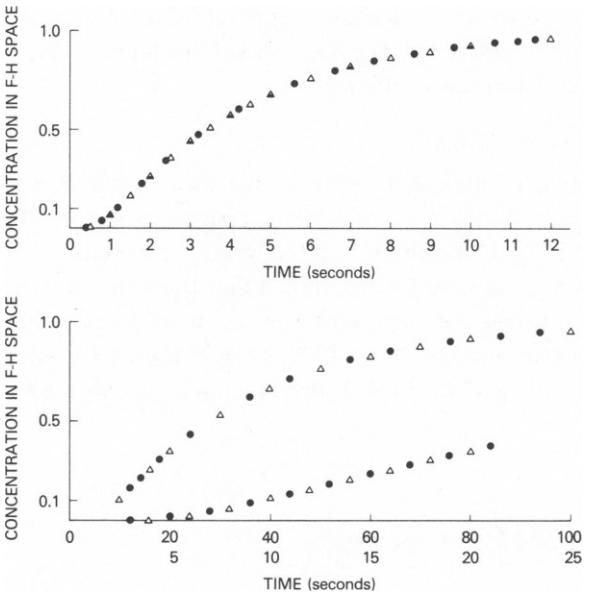

FIGURE 2 Concentration in the F-H space after a sudden change in external concentration for two sets of parameters using the anatomical model with convergence (Δ) (obtained by numerical inversion of Eq. 23) and without (●) (obtained by numerical solution of Eqs. 33–43). The parameters for the upper graph were: $k = 1$, $D_1 = D_2 = D_3 = D = 1.16 \times 10^{-5}$ cm^2/s; $a_1 = b_3 = 2$ μm; $a_2 - a_1 = 3$ μm; $a_3 - a_2 = 102$ μm; $b_2 = 60 \times 10^{-8}$ cm; $b_1 = 200 \times 10^{-8}$ cm. For the lower graph: $k = 1$, $D_1 = D_2 = D_3 = D = 1.16 \times 10^{-5}$ cm^2/s; $a_1 = b_3 = 4$ μm; $a_2 - a_1 = 7$ μm; $a_3 - a_2 = 270$ μm; $b_2 = 150 \times 10^{-8}$ cm; $b_1 = 300 \times 10^{-8}$ cm. The filled triangles in the upper graph were computed using the analytical solution (Eq. 52) for the model with thin membrane plus unstirred layer (see Fig. 7) using $P = 10.052 \times 10^{-5}$ cm/s. The two sets of points are plotted in two different time scales indicated in the abscissa.

complete curves and checked at selected points by summing to 500 or 700 terms. In none of the cases that we considered did the summation of Eq. 27 matter very much, i.e., it could be considered to be zero without significantly changing the result. This summation appears in the process of taking the Fourier transform with respect to y of the Laplace transform of Eq. 17 and its insignificance is a direct indication that convergence into the clefts from the unstirred layer is unimportant.

To illustrate the effect of the unstirred layer the results of computations using the anatomical model with convergence are shown by the crosses in Fig. 2 for two sets of anatomical parameters. Here the concentration in the F-H space (initially zero) is plotted against the time after a sudden change in the concentration externally from 0 to 1.0. Note that the half-time for filling is ~3.5 in the upper and ~28 s in the lower graph. This difference is almost entirely due to the change in the thickness of the unstirred layer.

ANATOMICAL MODEL: NO CONVERGENCE, BUT CHEMICAL REACTION AND BINDING

For this model we divided the shaded area in Fig. 1 into four regions, namely, 1 representing the F-H space, from $x = 0$ to $x = a_1$, of thickness b_1 (the distance between clefts is clearly $2a_1$); region 2 with a length $a_2 - a_1$ and width b_2 (cleft width is $2b_2$). The value of b_{3A} could be taken as different from b_{3B} to include the effect of some volume of connective tissue and/or basement membrane which was nonconducting or not available for diffusion. Region 3A is also distinguished from region 3B by the possibility of including nonsaturable binding sites in region 3A or a different diffusion coefficient.

Region 1: The F-H Space

Here we are interested in sites that occur on the axon membrane and bind saxitoxin or tetrodotoxin specifically. Since $b_1 \ll a_1$ we can assume mixing in the y direction and, as suggested to us by Sir A. L. Hodgkin in 1971 when the experimental work was done (see Rojas, 1973), it is valid to assume for calculation that these sites are distributed uniformly in the F-H space and we call their concentration n, in moles per cubic centimeter. In the presence of a certain concentration C_1 of TTX, some of these sites will be occupied (y_m) and an amount ($n - y_m$) will be unoccupied. If this binding is described by a first-order reaction:

$$C_1 + (n - y_m) \underset{k_2}{\overset{k_1}{\rightleftharpoons}} y_m, \tag{28}$$

with rate constants k_1 and k_2. At equilibrium,

$$K = \frac{k_2}{k_1} = \frac{C_1(n - y_m)}{y_m}, \tag{29}$$

and in general the rate of binding is:

$$\frac{\partial y_m}{\partial t} = k_1[C_1(n - y_m) - Ky_m] \equiv Y, \tag{30}$$

which defines Y.

The rate at which TTX is being bound by nonsaturable binding sites unrelated to the

sodium channels is $B_1 \partial C_1/\partial t$, where B_1 is the binding constant. The diffusion equation for this region, including the two types of binding is:

$$\frac{\partial C_1}{\partial t} = D_1 \frac{\partial^2 C_1}{\partial x^2} - B_1 \frac{\partial C_1}{\partial t} - Y, \tag{31}$$

which can be written as:

$$\frac{\partial C_1}{\partial t} = \frac{D_1}{(1 + B_1)} \frac{\partial^2 C_1}{\partial x^2} - \frac{Y}{(1 + B_1)}. \tag{32}$$

Thus the effect of the nonsaturable binding is to decrease the apparent diffusion coefficient by the factor $1/(1 + B_1)$. Define $D_1' = D_1/(1 + B_1)$ and $Y' = Y/(1 + B_1)$ and we have, for region 1,

$$\frac{\partial C_1}{\partial t} = D_1' \frac{\partial^2 C_1}{\partial x^2} - Y'. \tag{33}$$

The boundary conditions are:

$$\partial C_1/\partial x = 0, \text{ at } x = 0, \tag{34}$$

$$-F_1 = b_1 D_1 \partial C_1/\partial x = b_2 D_2 \partial C_2/\partial x, \text{ at } x = a_1, \tag{35}$$

where $-F_1$ is the total flow of TTX into the F-H space from region 2 (the cleft), and D_2 is the diffusion coefficient of the toxin in region 2.

Region 2: The Cleft between Schwann Cells

With only nonsaturable binding sites in the cleft of binding constant B_2 we have:

$$\partial C_2/\partial t = D_2' \partial C_2/\partial x^2, \tag{36}$$

where $D_2' = D_2/(1 + B_2)$ and the conditions

$$-F_1 = b_2 D_2 \partial C_2/\partial x = b_1 D_1 \partial C_1/\partial x, \text{ at } x = a_1, \tag{37}$$

$$-F_2 = b_2 D_2 \partial C_2/\partial x = b_{3A} D_{3A} \partial C_{3A}/\partial x, \text{ at } x = a_2, \tag{38}$$

where D_{3A} is the diffusion coefficient in 3A.

Region 3A: The Basement Membrane and Connective Tissue

Similar to region 2 with nonsaturable binding constant B_3, we have

$$\partial C_{3A}/\partial t = D_{3A}' \partial C_{3A}/\partial x^2, \tag{39}$$

where $D_{3A}' = D_{3A}/(1 + B_3)$, and

$$-F_2 = b_{3A} D_{3A} \partial C_3/\partial x = b_2 D_2 C_2/\partial x, \text{ at } x = a_2, \tag{40}$$

$$-F_3 = b_{3A} D_{3A} \partial C_{3A}/\partial x = b_{3B} D_{3B} \partial C_{3B}/\partial x, \text{ at } x = a_{3A}. \tag{41}$$

Region 3B: The Unstirred Layer

With no binding of any kind we have:

$$\partial C_{3B}/\partial t = D_{3B}\partial C_{3B}/\partial x^2, \tag{42}$$

$$-F_3 = b_{3B}D_{3B}\partial C_{3B}/\partial x = b_{3A}D_{3A}\partial C_{3A}/\partial x, \text{ at } x = a_{3A}, \tag{43}$$

$C_{3B}(a_{3B}, t) = c_a$, the external applied concentration.

A number of computations were made using this model (anatomical model without convergence) including specific and nonspecific binding in the F-H space and nonspecific binding in the clefts for comparison with experimental results on the time-course of the effects of TTX and STX (see Rojas, 1973; Keynes et al., 1975). Because of the large number of adjustable parameters and the fact that the predictions of the model are comparable to those using the thin membrane plus unstirred layer (see below), the latter model was preferred. For comparisons with experimental data using TTX and STX the reader is referred to previous papers (Rojas, 1973; Keynes et al., 1975). Here we present the results of calculations of the changes in concentration in the F-H space after a step change in external concentration.

Figure 2 shows the lack of effect of diffusion convergence into the clefts. The concentration in the F-H space after a sudden change in external concentration is plotted for the model with the convergence and without for two sets of parameters. No binding was assumed for these calculations.

Figure 3 illustrates the lack of effect of the thickness of the unstirred layer for the F-H experiment, i.e., the after effects of repetitive activity. Here the F-H space is initially loaded (concentration = 1.0) and drains through the clefts into an unstirred layer of thickness either 15 or 100 μm. The maximum difference was 0.000339 at 82 ms.

F-H MODEL AS LIMIT OF ANATOMICAL MODEL WITHOUT UNSTIRRED LAYER

Having compared the calculated concentration changes in the F-H space with and without diffusion convergence we consider the possibility of treating the model proposed by Frankenhauser and Hodgkin (1956) as a limiting case of the anatomical model.

The anatomical model that we have considered consists of a small, well-stirred space separated from the external unstirred layer by the communicating clefts. For the type of experiment analyzed originally by Frankenhauser and Hodgkin (1956) we have also found that the model that they used, i.e., a thin, well-stirred space bounded by an equivalent membrane with no unstirred layer, is satisfactory. For experiments where the sodium concentration in the external solution is suddenly varied and the time-course of the sodium concentration at the membrane surface is deduced from voltage clamp data (Rojas, 1973; Keynes et al., 1975), the addition of an external unstirred layer is necessary, but the clefts can still be replaced by an equivalent membrane. We will now consider the question of the conditions under which the clefts in the anatomical model may be replaced by a membrane.

To estimate a value for the length of cleft which would make the approximation valid, we considered a problem for which the solution is given by Carslaw and Jaeger (1947) for the temperature distribution in a slab with one face in contact with a layer of perfect conductor

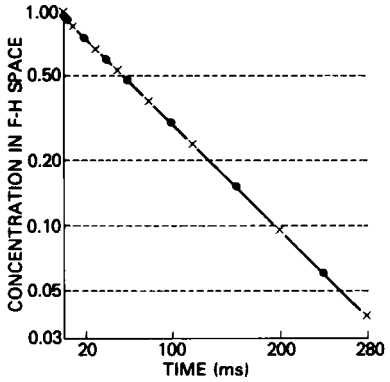

FIGURE 3

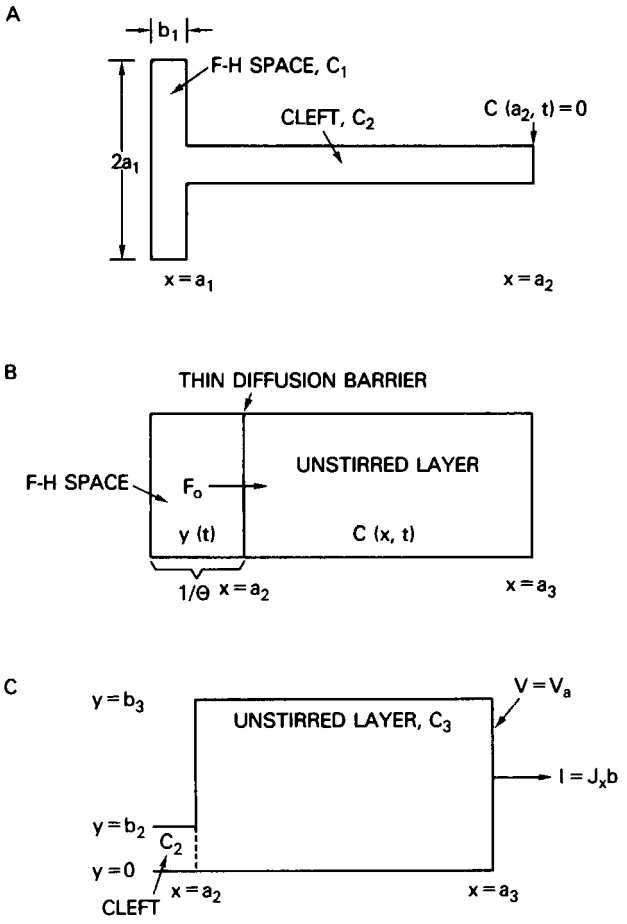

FIGURE 4

FIGURE 3 Comparison of computed results for the concentration in the F-H space $C_1(t)$ after an initial loading of this space using the anatomical model without diffusion convergence (Eqs. 33–43) for an unstirred layer of thickness $a_3 - a_2$ of 100 μm (●) and 15 μm (×). The parameters used were $D = 1.0 \times 10^{-5}$ cm^2/s; $a_1 = b_{3A} = b_{3B} = 6.5$ μm; $a_2 - a_1 = 5$ μm. Note that the straight line drawn through the dots at long times does not extrapolate to 1.0 at time zero.

FIGURE 4 (A) Anatomical model without unstirred layer. (B) Diagram of model where the clefts between the Schwann cells are replaced by an equivalent thin membrane and the effects of the unstirred layer are included. (C) Diagram to indicate the terms used in the calculation of series resistance including convergence into clefts from unstirred layer.

with a given initial temperature. The other face of the slab is maintained at zero temperature and initially the slab is at zero temperature. This corresponds in our case to an initial concentration in the well-stirred F-H space (the perfect conductor) of c_1 and a concentration in the clefts (the slab) of $C_2(x, t)$, where $C_2(a_2, t) = 0$ and $C_2(x, 0) = 0$. Here $x = a_2$ represents the outer end of the cleft (Fig. 4 A). We introduce D, the diffusion coefficient, in place of their K, and their h in our case is the ratio of the cross sectional area of the cleft to the volume of the

F-H space. The length of the cleft is $a_2 - a_1 = \ell$. We may write their solution as:

$$\frac{C_2(x,t)}{c_1} = \sum_{n=1}^{\infty} \frac{2 \exp \frac{-\alpha_n^2 Dt}{\ell^2} \sin \alpha_n \frac{a_2 - x}{\ell}}{\sin(\alpha_n)[\alpha_n(\tan \alpha_n + 1/\tan \alpha_n) + 1]}, \tag{44}$$

where the α_n are given by the roots of $\alpha \tan \alpha = h\ell$.

If the clefts are long, or what amounts to the same thing, the F-H space volume is very small, and the total quantity per square centimeter of membrane of extra initial loading is Q, then the initial concentration, $C_1(0) = Q/b_1 = Qh\, a_1/b_2 \equiv . C_2(a_1, 0)$.

As the volume of the F-H space approaches zero, h approaches infinity. In the expression above (Eq. 44), as h becomes very large the α_n approach $\pi(2n - 1)/2$. We thus have, at $x = a_1$,

$$\lim_{h \to \infty} C_2(a_1, t) = \lim_{h \to \infty} \frac{a_1}{b_2} \sum_{n=1}^{\infty} \frac{2Qhe^{-(2n-1)\pi^2 Dt/4\ell^2}}{h\ell + \alpha_n^2/h\ell + 1}, \tag{45}$$

$$\lim_{h \to \infty} C_2(a_1, t) = \frac{2Qa_1}{\ell b_2} \sum_{n=1}^{\infty} e^{-(2n-1)\pi^2 Dt/4\ell^2}. \tag{46}$$

If $a_1 = b_2$ (i.e., if the entire surface area is available for diffusion) this is Eq. 9*b* of Frankenhaeuser and Hodgkin (1956), i.e., their "hypothesis 2: finite diffusion barrier and no space," which did not fit their data.

In the case where the clefts are short and $\ell = a_2 - a_1$ approaches zero the time constant goes to zero. However, if we make the constraint that D/ℓ remains constant this quantity will be proportional to the permeability (P) of the thin membrane approximation. We note that the limit of $\alpha_n \tan \alpha_n$ is 0 for any n; the limit of $\alpha_n/\tan \alpha_n$ is 1 for $n = 1$ and infinite for $n > 1$; the limit of $\alpha_n D/\ell^2 = hD/\ell$ if $n = 1$ and infinite if $n > 1$. We finally arrive at:

$$\lim_{\ell \to 0} C_2(a_1, t) = c_1 e^{-hDt/\ell}. \tag{47}$$

If we define the P in terms of 1 cm^2 of cross section of the nerve membrane we see that $P/b_1 = hD/\ell$, where b_1 is the thickness of the F-H space. The concentration in the F-H space after an initial loading declines as e^{-Pt/b_1}, which is the same as "hypothesis 1: finite space and very thin barrier to diffusion" of Frankenhaeuser and Hodgkin (1956).

The final question is, How large can ℓ, the cleft length, be and still have the first term in the summation above dominate the series (Eq. 44)? By definition the sum of the series for $x = a_1$ and $t = 0$ is 1. The coefficient of the first term we will call A_1 and is a function only of $h\ell$, the ratio of the volume of the cleft to the volume of the F-H space. A more or less standard set of values that we have arrived at (Keynes et al., 1975) for Plymouth squid axons is a thickness of the F-H space and width of cleft of 300 Å and the clefts 13 μm apart. This gives $h = 1/(13 \times 10^{-4})cm^{-1}$. Fig. 5 shows a plot of A_1 vs. either ℓ or $h\ell$ (the ratio of the volume of the cleft to the volume of the F-H space). For A_1 to be > 0.9, $h\ell$ must be < 0.3, or, for our standard values, $\ell < 4$ μm. We consider this result to be quite satisfactory.

We can further ask about the time constant of the first term (τ_1) in the series (Eq. 44), which is ℓ^2/D_1^2, where $\alpha_1 \tan \alpha_1 = h\ell$. This quantity is also plotted in Fig. 5 for $D = 10^{-5}cm^2/s$.

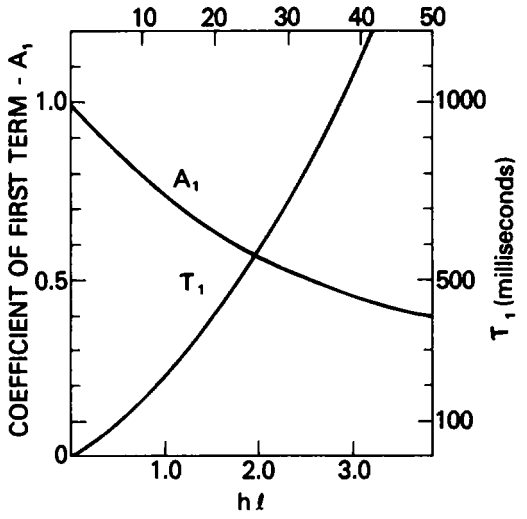

FIGURE 5 Coefficient and time constant of first term of concentration in F-H space as described in the text (Eq. 44) as a function of $h\ell$ and of ℓ for $1/h = 13$ μm, $D = 10^{-5}$ cm^2/s. Cleft length, ℓ (μm).

For $h\ell = 5/13$, i.e., $\ell = 5$ μm, the time constant is 73.53 ms, which is again a very satisfactory result. If the first term of the series is to dominate, $h\ell$ and thus α must be small. For a given $h\ell$ the time constant is proportional to ℓ^2.

For the limiting case where ℓ is small we arrived at a time constant of ℓ/hD. For $\ell = 5$ μm, $1/h = 13$ μm, and $D = 10^{-5}$cm^2/s, this time constant is 65 ms.

We conclude that the thin membrane approximation to represent the clefts happens to be reasonably good because the geometry happens to be appropriate. If the quantity $h\ell$ were very small there would be very little accumulation, and the problem would probably not have arisen in the first place. If $h\ell$ were large the thin membrane would not be a good approximation.

THIN DIFFUSION BARRIER WITH UNSTIRRED LAYER

A. No Binding: Numerical and Exact Solution

We have seen that in many cases the clefts between the Schwann cells may be represented by an equivalent thin membrane which separates the external unstirred layer from the F-H space (Rojas, 1973; Keynes et al., 1975). The model shown in Fig. 4 B was our first and is probably the most useful of all of the models which we have considered because it is relatively simple and appears to be a good approximation. In this discussion we will assume that the F-H space is well stirred, has a volume, V, and a concentration, $y(t)$. The clefts between the Schwann cells are represented by the thin membrane of area A and permeability P situated at $x = a_2$. The unstirred layer extends from $x = a_2$ to $x = a_3$ with a concentration of $C(x, t)$ of a substance with diffusion coefficient D.

With $L = a_3 - a_2$ for the unstirred layer we have:

$$\partial C/\partial t = D\partial^2 C/\partial x^2; \quad 0 < x < L \text{ (with } a_2 = 0). \tag{48}$$

The boundary condition at $x = L$ is

$$C(L, t) = C_L.$$

The boundary conditions at $x = 0$ are:

$$-D\mathrm{d}C/\mathrm{d}x = F_0, \tag{49}$$

the membrane flux,

$$F_0 A/V = \mathrm{d}y/\mathrm{d}t. \tag{50}$$

$$\mathrm{d}y/\mathrm{d}t = (PA/V)[C(0, t) - y], \tag{51}$$

and the initial conditions are:

$$y(0) = y_0,$$

$$C(L, 0) = C_{L0},$$

$$C(x, 0) = C^0.$$

These equations were solved by computer using a standard numerical approximation method. We present here an exact solution to this problem although the numerical approximation procedure appeared to be much more convenient to use.

We consider the case where the concentration in the F-H space at time zero is $y(0) = y_0$ and the concentration in the unstirred layer is $C(x, 0) = C^0$, and we suddenly change the concentration in the external region to $C(L, 0) = C_{L0}$. Application of the Laplace transform with respect to t to the above equations under these conditions and inverting the resulting transform for $y(t)$ by contour integration gives:

$$y(t) = y_0 e^{-P\theta t} + C_{L0}(1 - e^{-P\theta t}) - 2C_{L0}P\theta \sum_{n=1}^{\infty} \frac{e^{-D\gamma^2 t} - e^{-P\theta t}}{\gamma_m Q(\gamma_m) \sin \gamma_m L}$$

$$+ 2P\theta C^0 \sum_{n=1}^{\infty} \frac{(P\theta - D\gamma_m^2) - P\gamma_m \sin \gamma_m L}{(P\theta - D\gamma_m^2)\gamma_m Q(\gamma_m) \sin \gamma_m L} (e^{-D\gamma_m^2 t} - e^{-P\theta t})$$

$$+ 2P\theta y_0 \sum_{n=1}^{\infty} \frac{P(e^{-D\gamma_m^2 t} - e^{-P\theta t})}{(P\theta - D\gamma_m^2)Q(\gamma_m)}, \tag{52}$$

where

$$Q(\gamma_m) = P + LP\theta - L\gamma_m^2 D + \frac{P\gamma_m^2(2D + PL)}{P\theta - \gamma_m^2 D}. \tag{53}$$

γ_m are the roots of:

$$\gamma \tan \gamma L = \frac{P\theta - \gamma^2 D}{P}, \tag{54}$$

and

$$\theta = A/V.$$

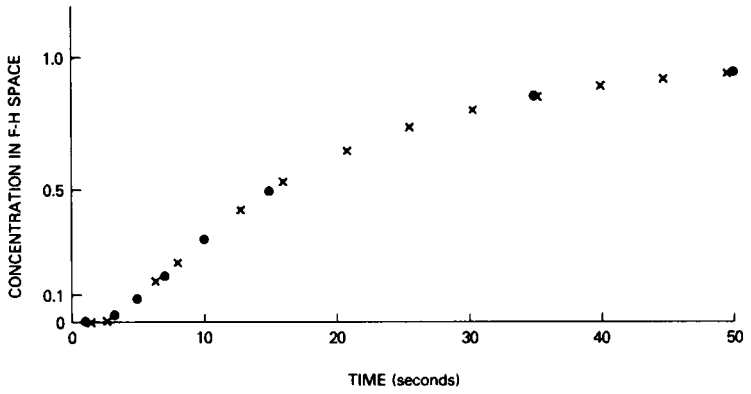

FIGURE 6 Concentration in the F-H space $y(t)$ after sudden change in external concentration. Comparison of computed results using numerical integration of Eqs. 48–51 (×) and analytical solution (Eq. 52) (●) for model with thin membrane plus unstirred layer. $P = 4 \times 10^{-5}$ cm/s; $D = 1 \times 10^{-5}$ cm^2/s; $a_3 - a_2 = L = 0.02$ cm; $1/\theta = 3 \times 10^{-6}$ cm.

The numerical solution and the analytical solution are compared in Fig. 6 for the concentration in the F-H space ($y(t)$ after a sudden change in the external concentration $C(L, t)$. The analytical solution was computed by summing the series involved to ~5 terms that gave an error <1 part in 10,000. The numerical solution corresponded to the analytical solution to 1 part in 1,000.

The model with thin membrane plus unstirred layer is much simpler than the anatomical model without convergence and we have compared some results of these models in Figs. 2 (top) and 7. In Fig. 2 the analytical model is compared to the anatomical model with and without convergence. For the parameters as shown in the figure legend the results are equal to within 1 part in 1,000.

The same parameters used for Fig. 2 were used to compute the concentration in the F-H space after an initial loading of this space as shown in Fig. 7. The dots and solid line are for the F-H model 1 (thin membrane with no unstirred layer); the squares are the solution of the analytical model using thin membrane plus unstirred layer and the crosses are for the anatomical model without convergence. For both Figs. 2 and 7 the permeability used for the thin membrane models was chosen to fit the time constant of the first term in the series solution for the model with F-H space plus cleft (Eq. 44) as shown in Fig. 3.

B. With Binding-Numerical Solution

The model used for the fitting of experimental results in Keynes et al. (1975) was the thin membrane with unstirred layer but including specific (saturating) and nonspecific binding of TTX or STX in the F-H space.

To incorporate binding into the expressions used in the previous section, we must add some definitions and change Eq. 51.

As we did for the anatomical model above we consider that the binding sites are uniformly distributed in the F-H space. The concentration of specific TTX or STX binding sites is n. In the presence of a TTX concentration, y, the number of sites bound will be y_m, and if the

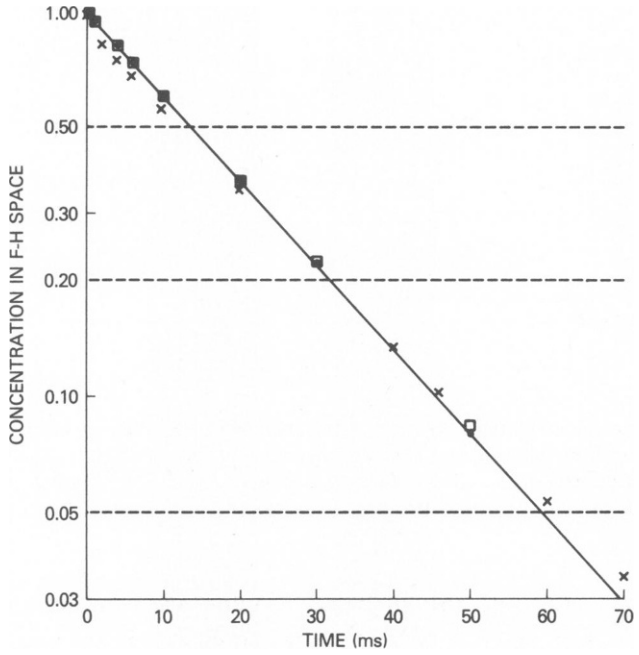

FIGURE 7 Concentration in the F-H space $y(t)$ after initial loading. Comparison of computed results using thin membrane (F-H model 1) (●), thin membrane plus unstirred layer, analytical solution (Eq. 52) (□), and anatomical model without convergence (Eqs. 33–43) (×). Parameters for the anatomical model without convergence are the same as those for Fig. 2 (top); for the thin membrane plus unstirred layer model the thickness of the F-H space ($1/\theta$), the thickness of the unstirred layer ($a_3 - a_2 = L$), and the D were also the same. The P is 10.052×10^{-5} cm/s and was chosen to make the time constant equal to that for the first term of the series (Eq. 44) applicable to the model shown in Fig. 4 A. The same P and F-H space thickness ($1/\theta$) were used for the thin membrane (F-H model 1). The solid line is drawn through the filled circles (F-H model 1).

binding is first order we get Eq. 28–30, again with y in place of C_1. The final equation is:

$$\frac{dy}{dt} = \frac{PA}{V(1 + B_1)}[C(0, t) - y] - \frac{Y}{(1 + B_1)}, \tag{55}$$

which replaces Eq. 51. The initial and boundary conditions remain the same. These equations were solved for y by numerical methods, and the results of these computations have been compared with the experimental data obtained in 1971 (Keynes et al., 1975).

SERIES RESISTANCE: EFFECTS OF CONVERGENCE INTO CLEFTS

We are interested in calculating the contribution of the external layers for any of the diffusion models to the resistance measured in series with the membrane. We shall present three ways of doing this for the models with convergence. For models without convergence the calculation is trivial.

A. Resistance between Ends of Strip with Abrupt Change in Width

For the geometry shown in Fig. 1 A we will neglect any contribution to the resistance due to the F-H space and first consider the remainder of the shaded area as a strip with abrupt

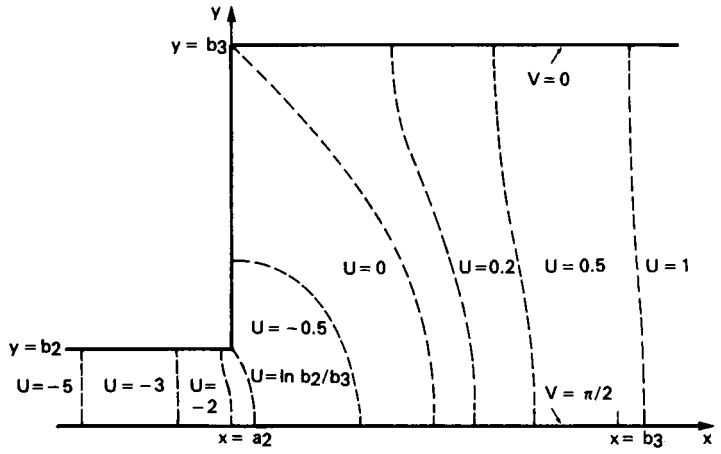

FIGURE 8 Outline (solid thick lines) and lines of constant potential (dotted lines) for current in a strip with abrupt change of width as calculated using Eq. 56. Here the ratio of the thin to the thick portions of the strip is taken to be 0.2, which is near the value at which the ratio of the convergence resistance to the cleft resistance is a maximum.

change in width. Half of the region near the junction between the cleft and the unstirred layer is shown in Fig. 8, with the strip lying along the x axis with width b_3 for $x > a_2$ and b_2 for $x < a_2$. Using the Schwarz-Christoffel transformation (Kober, 1957) it is possible to solve Laplace's equation for the flow of current in this region and construct lines of current flow and constant potential. Writing

$$Z = y + jx, j = \sqrt{-1},$$

$$W = U + jV,$$

where x and y are the coordinates shown in Figs. 4 C and 8. U = const is a line of constant potential and V = const is a line of current flow; the solution for an infinite strip is (Smythe, 1939):

$$Z = \frac{2}{\pi}\left[b_3 \tan^{-1}\left(\frac{e^{2W} - a^2}{1 - e^{2W}}\right)^{1/2} + b_2 \tan^{-1} a\left(\frac{1 - e^{2W}}{e^{2W} - a^2}\right)^{1/2}\right], \tag{56}$$

where

$$a = b_2/b_3.$$

Since, for any u, $\tan^{-1} ju = j \tan h^{-1} u$, and on the x axis $V = \pi/2$, for $y = 0$:

$$x = \frac{2}{\pi}\left[b_3 \tanh^{-1}\left(\frac{e^{2U} + a^2}{1 + e^{2U}}\right)^{1/2} - b_2 \tanh^{-1} a\left(\frac{1 + e^{2U}}{e^{2U} + a^2}\right)^{1/2}\right] + a_2. \tag{57}$$

If the narrow part of the strip has a length x_c and the wide part a length x_u and the resistivity of the strip material is σ, then the total resistance can be written as:

$$R = \sigma x_c/2b_2 + \sigma x_u/2b_3 + \Delta R.$$

Under the approximation that x_c and x_u are large, and e^{2U} is large compared to 1, a, and a^2, we can rearrange Eq. 5 (p. 232) of Smythe (1939) to give:

$$\Delta R = \frac{\sigma}{2\pi}\left[\left(\frac{1}{K} + K\right)\ln\left(\frac{K+1}{K-1}\right) - 2\ln\left(\frac{4K}{K^2-1}\right)\right], \tag{58}$$

where

$$K = b_3/b_2 = 1/a.$$

Note that R is a function only of σ and K and has the units of ohmcm/cleft. If we call r the resistance per square centimeter, and there are n clefts per centimeter then $r = R/n$ and $2b_2 = 1/n$.

The result is directly applicable to the model considered in Fig. 1 if the cleft length and the unstirred layer thickness are great enough that the lines of constant potential are virtually straight near the ends. Computation of lines of current flow and constant potential for the exact expression shows that "large" values are in the range $x_c > b_2$ and $x_u > b_3$. Lines of constant potential are shown in Fig. 8 for $K = 5$.

We thus have the series resistance in ohm per cm^2

$$r = R/n = 2b_3R = \sigma K x_c + \sigma x_u + 2b_3\Delta R. \tag{59}$$

The contribution of the clefts (r_c) and unstirred layer (r_u), ignoring convergence would be $r_c = \sigma K x_c = \sigma b_3 x_c/b_2$ and $r_u = \sigma x_u$, respectively.

To consider a specific example in the range of the experimental results using *Loligo vulgaris*, take the clefts to be 5 μm long and 400 Å wide spaced 10 μm apart with an unstirred layer of 200 μm and σ for sea water 26 Ωcm. The total series resistance is then $r = 3.250 + 0.520 + 0.04249898\ \Omega\text{cm}^2 = 3.81249898\ \Omega\text{cm}^2$.

The convergence resistance ($\Delta r = 2b_3\Delta R$, in Ωcm^2) in this case is small compared to the cleft resistance ($\Delta r/r_c = 0.01308$) and small compared to the unstirred layer resistance ($\Delta r/r_u = 0.08173$), and we take this to strengthen the validity of the approximations which we used for the diffusion equation solutions.

The convergence resistance is unlikely to ever be a large fraction of the cleft resistance. For example, with the values given above, the cleft width would have to be 1.34×10^{-4} cm to give the maximum possible $\Delta r/r_c = 0.16$. This value for cleft width is unrealistically big. Similarly, the convergence resistance is small compared to the unstirred layer resistance. It increases as the cleft becomes very narrow, but to get $\Delta r/r_u = 0.18$ the cleft width would have to be decreased to 10^{-8} cm (1.0 Å!).

The actual measured resistance could be less than calculated here because the voltage measuring electrodes must surely be able to penetrate some of the unstirred layer.

B. Convergence in Unstirred Layer into Cleft: First Method

The region external to the Schwann cells shown in Fig. 1 is represented as in Fig. 4 C. The line at $x = a_2$ from $y = 0$ to $y = b_2$ is considered the mouth of the cleft and we ask for the resistance between this line and the line at $x = a_3$ from $y = 0$ to $y = b_3$, assuming no flow of current across any other boundary. The resistivity of the region is equal to σ.

If V is the electrical potential at any point x, y, we have Laplace's equation, i.e.,

$$\frac{\partial^2 V}{\partial x^2} + \frac{\partial^2 V}{\partial y^2} = 0. \tag{60}$$

Assuming that at $x = a_3$ the potential is independent of y and is equal to V_{a_3} we can take the x component of the current density J as J_x and calculate the total current $I = J_x(a_3, y) \cdot b_3 \equiv J_x b_3$. We will assume that the current density along the line of the cleft mouth to be uniform and equal to $J_x b_3 / b_2$. We have the continuity conditions,

$$\left.\frac{\partial V}{\partial y}\right|_{y=0} = 0, \quad \left.\frac{\partial V}{\partial y}\right|_{y=b_3} = 0, \tag{61}$$

$$\left.\frac{\partial V}{\partial x}\right|_{x=a_2} = \begin{cases} -J_x b_3 \sigma / b_2, & 0 < y < b_2, \\ 0, & y > b_2. \end{cases} \tag{62}$$

Applying the Fourier transform to Eq. 1 with the kernel

$$\sqrt{\frac{2}{b_3}} \cos\left(\frac{m\pi y}{b_3}\right) \mathrm{d}y, \quad m = 1, 2, 3, \ldots,$$

we have

$$\int_0^{b_3} \left(\frac{\partial^2 V}{\partial x^2} + \frac{\partial^2 V}{\partial y^2}\right) \sqrt{\frac{2}{b_3}} \cos\left(\frac{n\pi}{b_3} y\right) \mathrm{d}y = 0. \tag{63}$$

With the Fourier transform of V with respect to y given by $\overline{V}$ we have

$$\frac{\mathrm{d}^2 \overline{V}}{\mathrm{d}x^2} - \frac{m^2\pi^2}{b_3^2} \overline{V} = 0; \; m = 1, 2, 3, \ldots$$

and (64)

$$\frac{\mathrm{d}^2 \overline{V}}{\mathrm{d}x^2} = 0; \; m = 0.$$

The solution of these equations is:

$$\overline{V} = \sigma \frac{J_x b_3^2}{b_2 m\pi} \sqrt{\frac{2}{b_3}} \cdot \sin \lambda b_2 \frac{\sinh \lambda(a_3 - a_2 - x)}{\lambda \cosh \lambda(a_3 - a_2)}, \; m = 1, 2, 3 \ldots, \tag{65}$$

where

$$\lambda = \frac{m\pi}{b_3}.$$

The inverse of this transform is:

$$V(x, y) = \sigma J_x (a_3 - a_2 - x) + V_a + \frac{2\sigma J_x b_3^2}{b_2 \pi^2} \sum_{m=1}^{\infty} \sin \lambda b_2 \cdot \frac{\lambda(a_3 - a_2 - x)}{m^2 \cosh \lambda(a_3 - a_2)} \cos \lambda y. \tag{66}$$

The average potential over the line $y = 0$ to $y = b_2$ at $x = a_2$ is given by:

$$\langle V(a_2)\rangle = \frac{1}{b_2}\int_0^{b_2} V(a_2, y)\,dy, \tag{67}$$

and the total current is $J_x b_3$. Thus we get a resistance of:

$$R = \frac{\langle V(a_2)\rangle - Va_3}{J_x b_3} = \sigma\left\{\frac{a_3 - a_2}{b_3} + \frac{2b_3^2}{b_2^2\pi^3}\sum_{m-1}^{\infty}\frac{\sin^2\dfrac{m\pi b_2}{b_3}\cdot\tanh\dfrac{m\pi(a_3 - a_2)}{b_3}}{m^3}\right\}. \tag{68}$$

We shall consider an example of computation of this resistance later.

C. Resistance Due to Convergence in Unstirred Layer into Cleft: Second Method

We consider the same region as in section B, but apply the Fourier transform with respect to x. We have Laplace's equation and the continuity conditions as in section B.

The Fourier transform of Laplace's equation with the kernel

$$\sqrt{\frac{2}{(a_3 - a_2)}}\cos\frac{(2m + 1)(x - a_2)}{2(a_3 - a_2)}$$

where the transform of V is $\overline{V}$ is

$$\frac{d^2\overline{V}}{dx^2} - \beta_m{}^2\overline{V} = \begin{cases} -P - Q, & y < b_2 \\ P, & y > b_2, \end{cases} \tag{69}$$

where

$$\beta_m = \frac{(2m + 1)\pi}{2(a_3 - a_2)},$$

$$P = \sqrt{\frac{2}{a_3 - a_2}}(-1)^m\beta_m V_a,$$

$$Q = \sigma\sqrt{\frac{2}{a_3 - a_2}}\cdot\frac{J_x b_3}{b_2}.$$

The inverse of this transform, evaluated at $x = a_2$ and $y < b_2$ is:

$$V(a_2, y) = \frac{\sigma J_x b_3}{b_2}\cdot\frac{2}{a_3 - a_2}\sum_{m-0}^{\infty}\frac{\sinh\beta_m(b_2 - b_3)}{\beta_m^2\sinh\beta_m b_3}\cosh\beta_m y + \frac{2}{a_3 - a_2}\sum_{m-0}^{\infty}\left\{\frac{(-1)^m}{\beta_m}V_a + \frac{\sigma J_x b_3}{b_2\beta_m^2}\right\}. \tag{70}$$

The resistance is:

$$R = \frac{\langle V(a_2)\rangle - V_a}{J_x b_3} = \sigma\left\{\frac{a_3 - a_2}{b_2} - \frac{16(a_3 - a_2)^2}{\pi^3 b_2^2}\sum_{m-0}^{\infty}\frac{\sinh\beta_m(b_3 - b_2)\sinh\beta_m b_2}{(2m + 1)^3\sinh\beta_m b_3}\right\}. \tag{71}$$

For the case $a_3 - a_2 = b_3$ and $b_2 = b_3/2$ Eqs. 68 and 71 can be evaluated explicitly using series summation tables (Selby, 1972) giving in both cases:

$$\frac{\langle V(a_2)\rangle - V_a}{J_x b_3} = 1.2704\sigma.$$

The infinite series that occur in Eqs. 68 and 71 converge slowly, but a good value for R can be obtained by evaluating only a few terms of each series. It can be seen from inspection that the series in Eq. 68 is added to $(a_3 - a_2)/b_3$, whereas the series in Eq. 71 is subtracted from $(a_3 - a_2)/b_2$. This means that the exact value of R always lies between the two values obtained from Eqs. 68 and 71 when only a few terms are evaluated.

For the examples $a_3 - a_2 = b_3$ and $b_2 = b_3/2$ Eq. 58 obtained using the Schwartz-Christoffel transformation, gives $\Delta R = 0.1249\sigma$. This number refers to a whole cleft so to compare with the result of Eqs. 68 and 71 for half a cleft we multiply by two and the total resistance $R = 2(0.1249)\sigma + 1.0\sigma = 1.2598\sigma$. This number is slightly smaller than the 1.2704σ from Eqs. 68 and 71, which is reasonable because of the approximation used for Eq. 58 that the lines of current flow are parallel at the outer edge of the unstirred layer (see Fig. 8).

D. Conclusions from the Three Ways of Analyzing the Effect of Convergence on Series Resistance

There are three conclusions that arise from the consideration of these models. The first is that we may neglect the effect of convergence into the clefts from the outer layers in the case of the series resistance. The second is that this provides strong support for the neglect of convergence into the clefts in the case of diffusion. The third is that the comparison of the three analyses gives strong support for the validity of the kinds of boundary conditions that were used in the diffusion models.

DISCUSSION

What we have referred to as the "anatomical model" here is the one shown by the shaded region of Fig. 1 A. This is already a severe simplification of the actual situation. More complicated models have been considered by us, in some detail in some cases, but the number of adjustable parameters involved in any comparison with experimental data can become very large. Our primary interest in the use of these models was to arrive at a number for the conductance of a single sodium channel in the squid axon membrane by measurements of the time-course of the effects of TTX and STX on the sodium currents during voltage clamping leading to a number for the density of sodium channels in the same axon for which the sodium current itself could be obtained (Rojas, 1973; Keynes et al., 1975). Because of the large number of adjustable parameters involved, it would be hopeless to try to fit all of them by only one type of experiment. Experiments were done to determine the time-course of the concentration of sodium in the F-H space after a sudden change of external sodium concentration. This was done by first measuring the steady-state relationship between external sodium concentration and peak sodium current and then determining the time-course of the peak sodium current after a sudden change of external sodium concentration. These experiments gave an estimate of the thickness of the unstirred layer. The after effects of

repetitive stimulation (the F-H experiments) gave an estimate of $P\lambda$ for the model of thin membrane plus unstirred layer. These results plus the morphology as determined by electron microscopy were used to fit the TTX experiments with the model containing the membrane plus unstirred layer with specific binding in the F-H space (Rojas, 1973; Bezanilla et al., 1973). A figure of 5 pS/cm^2 for single channel conductance was obtained (Keynes et al., 1973). Later, unspecific binding was incorporated into this model and the results were presented by Keynes et al. (1975).

The most complete model to represent the shaded area in Fig. 1 A would be the anatomical model including the effect of convergence into the clefts from the unstirred layer and, for the TTX experiments, the effects of specific and nonspecific binding. In practice this was simplified. As discussed above (see Fig. 1 C) the effects of convergence from the unstirred layer into the cleft can be ignored both for the diffusion and the series resistance. It should be stated again that the replacement of the clefts by a thin membrane would not work in all cases but only when the geometry was appropriate.

In spite of the very complicated geometry involved in the study of diffusion of ions through the Schwann cell layer of the squid giant axon, simplified models appear to be adequate in certain cases. We have considered the properties of these models here and have concluded the following.

(*a*) The effects of convergence into the mouths of the clefts from the outside can be neglected both for diffusion and for calculation of series resistance. (*b*) For those experiments involving the time-course of potassium ion concentration in the F-H space after an initial loading, the effects of the external unstirred layer may be neglected. In this case the clefts are rate limiting and may be replaced by a thin membrane with good accuracy at long times. At short times small differences occur. (*c*) For those experiments involving the time-course of concentration in the F-H space after changes in external concentration the unstirred layer is rate limiting. The clefts may be neglected in this case except for short times. The model in which the clefts are replaced by an equivalent thin membrane is accurate at all times.

In the use of these models for fitting experimental data on the time-course of the effects of TTX or STX (Keynes et al., 1975) the thin membrane plus unstirred layer with specific and nonspecific binding in the F-H space was employed.

We would like to thank Dr. Julio Vergara and Dr. Richard FitzHugh for their help in some of the computations and Dr. Richard S. Eisenberg for reading an early version of the manuscript.

Received for publication 18 April 1978 and in revised form 26 September 1979.

REFERENCES

ADAM, G. 1973. The effect of potassium diffusion through the Schwann cell layer on potassium conductance of the squid axon. *J. Membr. Biol.* **13**:353–386.

ADELMAN, W. J., JR., Y. PALTI, and J. P. SENFT. 1973. Potassium ion accumulation in a periaxonal space and its effect on the measurement of membrane potassium ion conductance. *J. Membr. Biol.* **13**:387–410.

BEZANILLA, F., E. ROJAS, and R. E. TAYLOR. 1973. Model for diffusion barriers in squid giant axons. *J. Gen. Physiol.* **61**:268. (Abstr.)

CARSLAW, H. S., and J. C. JAEGER. 1947. Conduction of heat in solids. Oxford University Press, Oxford, England. pp. 386.

FRANKENHAEUSER, B., and A. L. Hodgkin. 1956. The after-effects of impulses in the giant nerve fibers of *Loligo*. *J. Physiol.* **131**:341–376.

GEREN, B. B., and F. O. SCHMITT. 1954. The structure of the Schwann cell and its relation to the axon in certain invertebrate nerve fibers. *Proc. Natl. Acad. Sci. U.S.A.* **40**:863–870.

GOLDMAN, L. 1968. The effects of some ions on the membrane potential of the giant axon of *Myxicola*. *J. Cell. Physiol.* **71**:33–42.

HODGKIN, A. L., and A. F. HUXLEY. 1952. The components of membrane conductance in the giant axon of *Loligo*. *J. Physiol. (Lond.)*. **116**:473–496.

KEYNES, R. D., F. BEZANILLA, E. ROJAS, and R. E. TAYLOR. 1975. The rate of action of tetrodotoxin on sodium conductance in the squid giant axon. *Philos. Trans. R. Soc. Biol. B. Biol. Sci.* **270**:365–375.

KEYNES, R. D., E. ROJAS, R. E. TAYLOR, and F. BEZANILLA. 1974. The rate of action of tetrodotoxin in the squid giant axon. *Disc. R. Soc. Lond.* 5. (Abstr.).

KEYNES, R. D., E. ROJAS, and R. E. TAYLOR. 1973. Saxitoxin, tetrodotoxin barriers, and binding sites in squid giant axons. *J. Gen. Physiol.* **61**:276. (Abstr.).

KOBER, H. 1957. Dictionary of conformational representations. Dover Publications, Inc., New York. 148–161.

LENNON, A. M., E. ROJAS, F. BEZANILLA, and R. E. TAYLOR. 1970. Diffusion of sodium and chloride ions in the extracellular spaces of squid giant axon. *Biophys. Soc. Abstr.* TPM-4.

ÖZIŞIK, M. N. 1968. Boundary value problems of heat conduction. Scranton, Pa. International Textbook Co., Ltd., London. pp. 505.

PAPOULIS, A. 1957. A new method of inversion of the Laplace transform. *Quart. J. Appl. Math.* **14**:405–414.

ROJAS, E., R. E. TAYLOR, I. ATWATER, and F. BEZANILLA. 1969. Analysis of the effects of calcium or magnesium on voltage clamp currents in perfused squid axons bathed in solutions of high potassium. *J. Gen. Physiol.* **54**:532–552.

ROJAS, E. 1973. The conductance of a single sodium channel in squid giant axons from *Loligo*. *Acta. Physiol. Lat. Am.* **23**:90–92.

SELBY, S. M., editor. 1972. Standard Mathematical Tables. 20th edition. The Chemical Rubber Co., Cleveland, Ohio.

SHANES, A. M., H. GRUNDFEST, and W. FREYGANG. 1953. Low level impedance changes following the spike in the squid giant axon before and after treatment with 'veratrine' alkaloids. *J. Pharmacol.* **37**:39–51.

SMYTHE, W. R. 1939. Static and dynamic electricity. McGraw-Hill Book Co., New York. pp. 560.

STEHFEST, H. 1970. Algorithm 368 numerical inversion of Laplace transforms [D5]. Communications of the Association for Computing Machinery. **13**:47.

TAYLOR, R. E., E. ROJAS, I. ATWATER, and F. BEZANILLA. 1969. Time course of membrane potential with changes of internal or external potassium in giant squid axons. *Biophys. Soc. Abstr.* SAM-H5. **9**:A-248.

VILLEGAS, G. M. 1969. Electron microscopic study of the giant nerve fiber of the giant squid *Dosidicus gigas*. *J. Ultrastruct. Res.* **26**:501–514.

VILLEGAS, R., and G. M. VILLEGAS. 1960. Characterization of the membranes in the giant nerve fiber of the squid. *J. Gen. Physiol.* **43**:73–103.

VILLEGAS, G. M., and R. VILLEGAS. 1960. The ultrastructure of the giant nerve fiber of the squid: Axon-Schwann cell relationships. *J. Ultrastruct. Res.* **3**:362–373.